Copyright © 2007 by ABCM

ANALYSIS OF EXTERNALLY PRESSURIZED GAS JOURNAL BEARING BY USING THE FINITE ELEMENT METHOD

Neves, Marcos Theiss, theiss@unifei.edu.br
Schwarz, Vilmar Arthur, vilmar@unifei.edu.br
Universidade Federal de Itajubá, Av. BPS 1303, Bairro Pinheirinho, Itajubá, MG

Menon, Genésio José, genesio@unifei.edu.br
Universidade Federal de Itajubá, Av. BPS 1303, Bairro Pinheirinho, Itajubá, MG

Abstract. *The solution of the compressible lubrication problem by applying the finite element method with linear triangular element is presented. Considerable work has been done to achieve better theoretical results by using several numerical techniques. The finite difference method is still being applied on gas journal bearing lubrication, even though this method is unsuitable for mesh refinement in localized areas of particular interest, such as near the supply holes where pressure gradients are high. In this work, the finite element method is used with special attention to local mesh refinement near the externally pressurized gas feeding holes, instead of refining the whole computational domain. With this approach, both the accuracy of the calculated bearing design parameters and reduced computational time were achieved. One of the most important conclusions is that the localized mesh refinement near the feeding holes resulted in a significant increase of the calculated pressure at the feeding holes and a reduction of the pressures on other grid points, as compared to the values obtained with standard domain discretization without localized refinements. Consequently the load carrying capacity is somewhat affected.*

Keywords*: tribology, gas journal bearing, finite element method, externally-pressurized, orifice-compensated.*

1. INTRODUCTION

The solution of compressible lubrication problems by numerical methods is of special importance, not only by the nonlinearity of the governing equation, but also due to the complexity of some bearing geometries. From this, numerical methods such as finite difference method-FDM, control volume method-CVM and finite element method-FEM are widely employed to solve some form of the generalized Reynolds equation for compressible lubrication problems. Over the past several years, finite difference method has been preferred for solving lubrication problems, although it has limitations mainly on dealing with some forms of bearing geometries and grid generation. The decomposition of the solution domain into an adequate mesh has always been done by the conventional uniform grid solution.

Nowadays, finite element method has been preferred, since it offers several advantages when applied to the lubrication problems. It can deal with complex bearing geometry, as well as with variations of the lubricant properties. Also, boundary conditions in terms of pressure or flow are simple to be prescribed. This work presents a theoretical analysis of the externally pressurized aerostatic journal bearing by FEM. The performance prediction of this type of bearing is undertaken with emphasis on the investigation about the decomposition of the solution domain and the mesh refinement near the feeding holes. This localized refinement showed to be necessary due to high pressure gradients over this region.

As mentioned on the classical publication by Powell (1970), on the 60´s there were virtually no externally pressurized aerostatic bearings used in Great Britain, apart from the pioneering research of G. L. Shires and Robinson & Sterry. Nowadays, this type of bearings is becoming more usual in engineering applications. Among all other features, such as high speed, low friction, precision of the axis definition, etc., they are environmentally safer as compared to oil lubricated bearings.

Reddi and Chu (1970) published the variational formulation for the solution of the compressible lubrication problem. The problem was reduced either to a set of nonlinear algebraic equations which could be solved by iteration or to a sequence of linear problems which could be solved by Gaussian elimination. Three thrust bearing geometries were analyzed through the same finite element computer program. Both direct and incremental variational formulations were presented and showed the advantages of the finite element approach in treating complex geometries and dealing with large pressure gradients.

Kazimierski and Trojnarski (1980) investigated the externally pressurized gas bearings with different feeding systems. A general calculation method for gas journal bearing with pocketed or annular orifices feeding systems was presented. The FDM was adopted as the numerical solution method with the conventional uniform grid solution. Examinations of the influence of the type of the feeding holes and of their dimensions on the non-dimensional load carrying capacity were performed. Comparisons between theoretical and experimental results were made and good agreement was found for an aerostatic journal bearing.

Majundar (1980) published a review of externally pressurized gas bearings. He mentioned the advantages, limitations and applications of such bearings under various design conditions. He emphasizes that design procedure for

gas bearing is similar to that for oil lubricated bearings; however the gas bearing shows additional complications owing to compressibility effects. He lists a series of papers which developed simplified theories and design charts for computing the performance of several types of gas bearings. On his conclusions, he comments that much information on the static behavior and stability characteristics is available, but little is known about the complicated flow phenomena near the supply holes.

Wadhwa, Sinhasan and Singh (1981), presented the steady state performance characteristics of pocket-type orifice-compensated bearings by using the FEM and extending the incremental formulation suggested by Reddi and Chu (1970). The validity of their studies was established in various test cases. The developed bearing surface was discretized by a set of isoparametric quadrilateral elements, but with a reduced number of elements and without any mesh refinement around the feeding holes. The unknown pressure over the isoparametric elements could take either the linear or parabolic variation.

Sorin et all (2003), presented a numerical scheme to solve compressible flows problems, which was entitled space-time conservation element and solution element (CE/SE) method. The method was applied to calculate mainly the pressure distribution of some gas journal bearings. The numerical results were compared with experimental data and good agreement between the computed and test data were found.

More recently, Cheng-Ying Lo et all (2005), evaluated the performance of an aerostatic journal bearing by using the finite difference method. They investigate the effects of the gas supply pressure, orifice diameter, gas film thickness and eccentricity ratio upon the load carrying capacity of the bearing.

2. MATHEMATICAL MODEL

2.1. The aerostatic journal bearing

Figure (1) shows the aerostatic journal bearing configuration, which is identical to the work published by Sorin et all (2003). Two sets of fourteen feeding holes are arranged evenly around the circumference of the journal bearing. Each set is located at 12.7 mm (L/9.25) from the bearing edges. Note that the radial clearance, c, the eccentricity, e, and the gas film thickness, h, are quite exaggerated, for clarity purposes. As usual, the bearing length and diameter are denoted respectively by L and D. The radial clearance c, is equal to half the difference between the bush and journal diameters. The bearing main dimensions and other characteristics are given in Tab. 1. Air properties are given in Tab. 2.

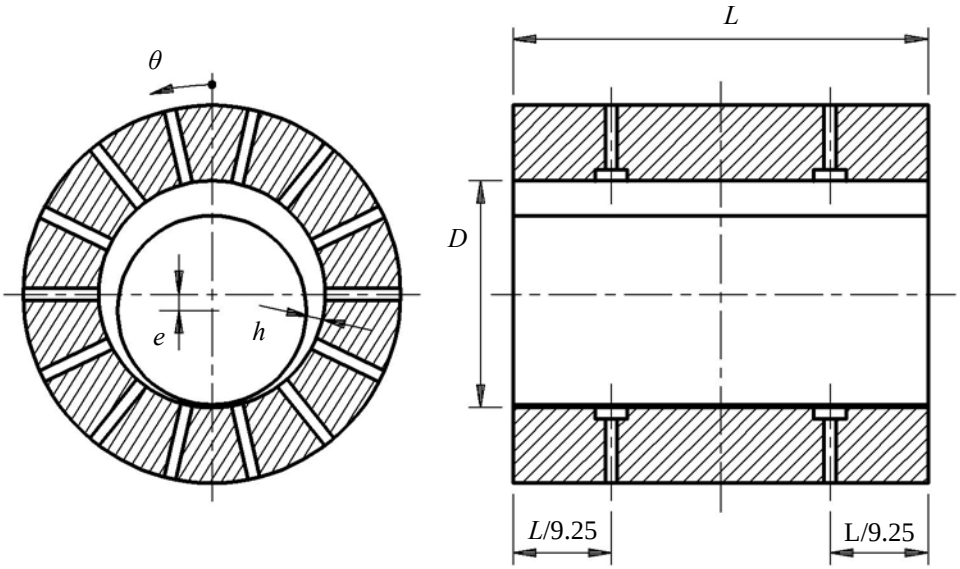

Figure 1. Aerostatic journal bearing configuration.

Figure (2) shows the computational domain of the aerostatic journal bearing and the applied periodic boundary condition, as well as a typical area (dashed) for mesh refinement around a feeding hole. For the purpose of direct comparison of the calculated pressure at any nodal point, the standard and the refined FEM meshes are generated by keeping the same FDM nodes coordinates. Obviously, several extra nodes must be created over the standard rectangular mesh in order to refine the area around each feeding hole.

In this paper, since the gas feeding holes act as punctual flow sources, several mesh refinement near the feeding holes are employed in order to investigate changes of the calculated pressure distribution and the load carrying capacity of an aerostatic journal bearing, as a function of these mesh refinements. As far as the authors' knowledge, this aspect has not yet been investigated.

Table 1 – Journal bearing dimensions and other operating characteristics.

Bearing length, L	117.5	*mm*
Bearing diameter, D	60.4	*mm*
Radial clearance, c	12.7	μm
Bearing eccentricity, ε	0.2	---
Rows of feeding holes	2	---
Feeding holes location from the bearing edges, $\left(\frac{L}{9.25}\right)$	12.7	*mm*
Feeding holes per row	14	---
Orifice diameter	0.16	*mm*
Pocket diameter	0.9	*mm*
Air supply pressure p_s (gauge)	0.5514	*MPa*

Table 2 – Air physical properties.

Atmospheric pressure, p_a	0.1013	*MPa*
Air specific mass, ρ_a	1.225	kg/m^3
Air absolute viscosity, μ	$1.781\ 10^{-5}$	*Pa.s*
c_p	1004	*J/(kg.K)*
c_v	717.4	*J/(kg.K)*
k	1.40	---

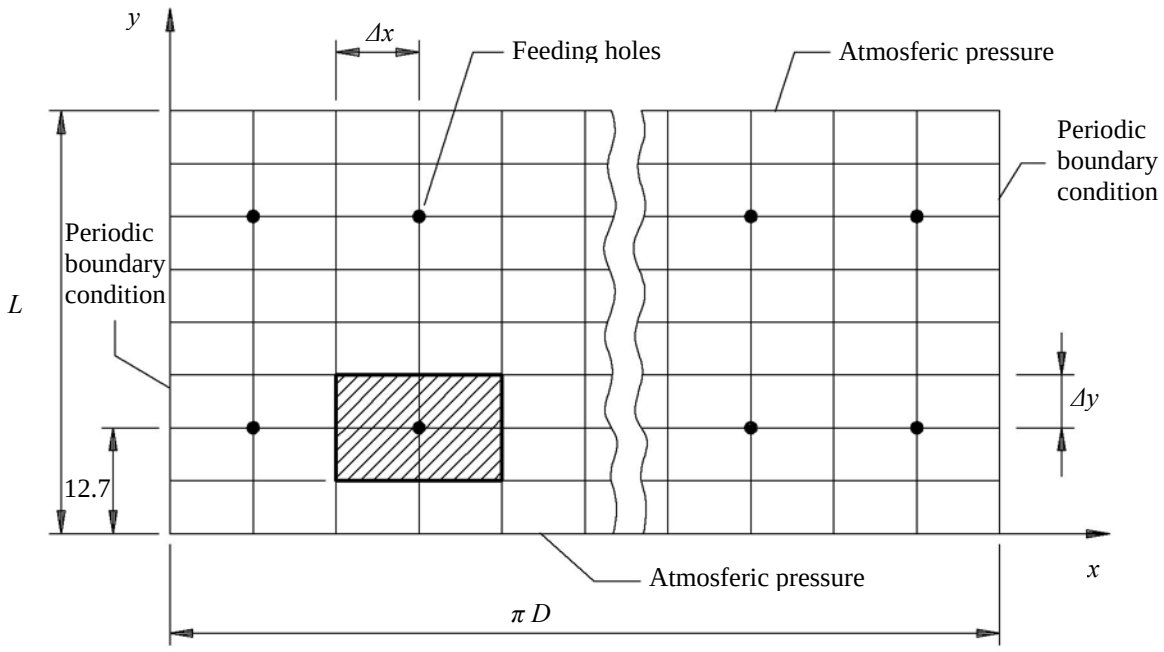

Figure 2. Computational domain of the aerostatic journal bearing.

2.2. Governing Equation and Finite Element Formulation

For compressible fluids and isothermal conditions, the Reynolds's equation is:

$$\frac{\partial}{\partial x}\left(h^3\frac{\partial p^2}{\partial x}\right)+\frac{\partial}{\partial y}\left(h^3\frac{\partial p^2}{\partial y}\right)=2\left\{6\mu U\frac{\partial(ph)}{\partial x}-12\mu\frac{p_a}{\rho_a}\int_0^h q\,dz\right\} \tag{1}$$

where p is the pressure, μ is the fluid viscosity, U is the tangential velocity, x and y are the circumferential and axial coordinates, h is the film thickness, p_a is the atmospheric pressure, ρ_a is the specific mass of the fluid and q is the mass per unit volume of fluid flowing out from a feeding hole per unit time. The film thickness h is given by:

$$h=c(1+\varepsilon\cos\theta) \tag{2}$$

where the dimensionless eccentricity $\varepsilon=e/c$, c is the radial clearance, R the bearing radius and e is the eccentricity.

For the case of an aerostatic journal bearing Eq. (2) simplifies to:

$$\frac{\partial}{\partial x}\left(h^3\frac{\partial p^2}{\partial x}\right)+\frac{\partial}{\partial y}\left(h^3\frac{\partial p^2}{\partial y}\right)=-24\mu\frac{p_a}{\rho_a}\int_0^h q\,dz \tag{3}$$

The computational domain, i.e. the developed bearing surface is discretized by using isoparametric linear triangular elements, as shown in Fig. 3 and Fig. 4.

The pressure distribution and its derivative are given by:

$$p^2=f=[N]\{F\}\;;\frac{\partial p}{\partial x}=\left(\frac{1}{2p}\right)\frac{\partial f}{\partial x} \tag{4}$$

where $[N]=\begin{bmatrix}N_i & N_j & N_k\end{bmatrix}$ is the vector shape function. These shape functions can be found in Baker (1991).

Substituting Eqs. (4) into Eq. (3) and employing Galerkin's technique leads to the following equation:

$$-\iint_\Omega [N]^T\left[\frac{\partial}{\partial x}\left(h^3\frac{\partial f}{\partial x}\right)+\frac{\partial}{\partial y}\left(h^3\frac{\partial f}{\partial y}\right)+24\mu\frac{p_a}{\rho_a}\int_0^h q\,dz\right]dx\,dy=0 \tag{5}$$

Assuming the film thickness is constant on each element, then Eq. (5) may be written as follows:

$$-\iint_\Omega\left[h^3[N]^T\frac{\partial^2 f}{\partial x^2}+h^3[N]^T\frac{\partial^2 f}{\partial y^2}+24\mu[N]^T\left(\frac{p_a}{\rho_a}\right)\int_0^h q\,dz\right]dx\,dy=0 \tag{6}$$

Employing the Green's theorem to Eq. (6) results:

$$\iint_\Omega\left[h^3\left\{\frac{\partial[N]^T}{\partial x}\frac{\partial f}{\partial x}\right\}+h^3\left\{\frac{\partial[N]^T}{\partial y}\frac{\partial f}{\partial y}\right\}-\oint_\Gamma h^3[N]^T\frac{\partial f}{\partial n}\vec{n}\,d\Gamma-[N]^T\,24\mu\frac{p_a}{\rho_a}\int_0^h q\,dz\right]dx\,dy=0 \tag{7}$$

If all the feeding holes positions coincide with node positions, then the shape function can be assumed as equal to unity at these points. Therefore, one can write:

Copyright © 2007 by ABCM

$$\int_0^h \iint_{\Delta I} N_i \, q \, dx \, dy \, dz \cong \int_0^h \iint_{\Delta I} q \, dx \, dy \, dz \tag{8}$$

Since Eq. (8) express the mass flow rate of fluid through the feeding hole, it is usual to use the equation for compressible flow through a nozzle, which is a function of supply and orifice discharge pressures.

$$\int_0^h \iint_{\Delta I} q \, dx \, dy \, dz = \frac{C_D \, A \, p_S}{\left(R \, T_S\right)^{\frac{1}{2}}} \, \Phi\left(p_i\right) \tag{9}$$

where C_D is the coefficient of discharge, A is the area of the feeding hole, R is the gas constant, T_s and p_s are the absolute temperature and absolute pressure of the air supply, respectively, and p_i is the discharge pressure at the feeding hole.

The function $\Phi\left(p_i\right)$ can be calculated either by Eq. (10) or Eq. (11), depending on the $\frac{p_i}{p_s}$ ratio, as follows:

$$\Phi\left(p_i\right) = \left[\frac{2}{(k-1)} \left(\frac{p_i}{p_s} \right)^{\frac{2}{k}} \left\{ 1 - \left(\frac{p_i}{p_s} \right)^{\frac{(k-1)}{k}} \right\} \right]^{\frac{1}{2}} \qquad \text{if} \qquad \frac{p_i}{p_s} \geq \left(\frac{2}{k+1} \right)^{\frac{k}{(k-1)}} \tag{10}$$

and

$$\Phi\left(p_i\right) = \left[k \left(\frac{2}{k+1} \right)^{\frac{(k+1)}{(k-1)}} \right]^{\frac{1}{2}} \qquad \text{if} \qquad \frac{p_i}{p_s} < \left(\frac{2}{k+1} \right)^{\frac{k}{(k-1)}} \tag{11}$$

where k is the gas specific heat ratio.

2.3. Method of solution

Equations (7) and (9) can be written in matrix form as follows:

$$\begin{bmatrix} a_{11} & a_{12} & \cdots & a_{1n} \\ a_{21} & a_{22} & \cdots & \vdots \\ \vdots & \vdots & \ddots & \vdots \\ a_{n1} & \cdots & \cdots & a_{nn} \end{bmatrix} \begin{Bmatrix} f_1 \\ f_2 \\ \vdots \\ f_n \end{Bmatrix} = \begin{Bmatrix} b_1 \\ b_2 \\ \vdots \\ b_n \end{Bmatrix} \tag{12}$$

where

$a_{ij} = \iint_{\Omega} h^3 \left(\frac{\partial N_i}{\partial x} \frac{\partial N_j}{\partial x} + \frac{\partial N_i}{\partial y} \frac{\partial N_j}{\partial y} \right) dxdy$, where Ω is the computational domain;

$$b_i = \begin{cases} 24\mu \dfrac{p_a}{\rho_a} \dfrac{C_D \, A \, p_s}{\left(R \, T_S\right)} \Phi\left(p_i\right) & \text{(if node } i \text{ is a feeding hole)} \\ 0 & \text{(if node } i \text{ is not a feeding hole)} \end{cases}$$

The linear system given by Eq. 12 must be calculated by an iterative method, since they contain the pressure itself and its derivative. The boundary conditions should be applied as follows:

- The nodes pressures at the bearing edges are equal to the atmospheric pressure;
- The periodic boundary condition is applied to nodes pressures at $x = 0$ and $x = \pi D$, i.e., $p_i(y)_{x=0} = p_i(y)_{x=\pi D}$.

The iterative method basic procedure is outlined as follows:

(1) The developed bearing surface is discretized, starting with the standard rectangular mesh of 57 x 38 equally spaced nodal points, respectively in *x* and *y* directions (mesh refinements will be later applied to the regions near the feeding holes);
(2) The boundary conditions are applied in Eqs. (7) and (9);
(3) Only for the first iteration, the pressures at all the other nodes are also assumed to be equal to ambient pressure;
(4) Solve Eq. (7) and obtain nodes pressures by using Eq. (4);
(5) Compare the new obtained pressures to the previous ones, and check for the convergence criterion;
(6) Update the pressures and repeat steps 4 to 7, until the required tolerance is achieved.
(7) Evaluate the load carrying capacity.

The procedure of the computer simulation is then repeated for the two types of mesh refinement around the feeding holes, as shown in Fig. 3 and Fig. 4. These types of mesh refinements are applied over the standard rectangular equally spaced mesh (see dashed region in Fig. 2). In this way, it will be possible to investigate the variation of the calculated pressure distributions and load carrying capacities of aerostatic journal bearings, for different types of mesh refinement around the feeding holes.

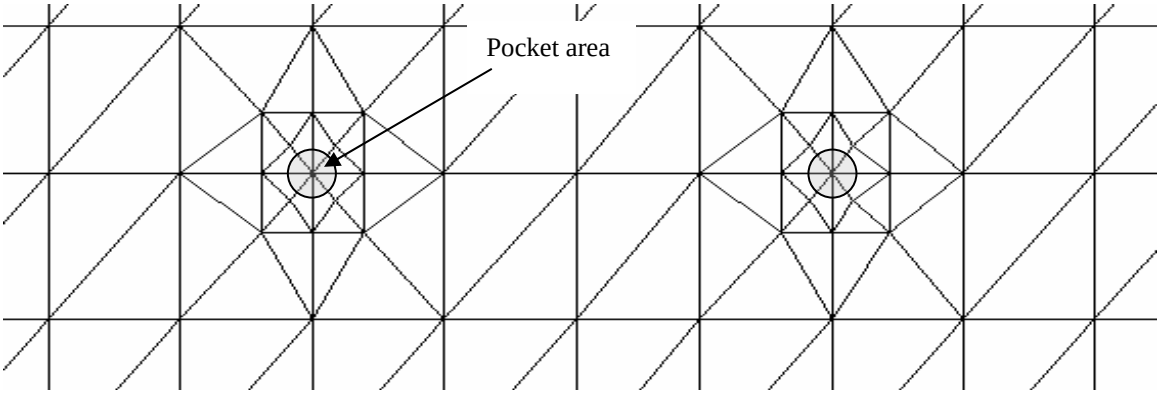

Figure 3. Mesh refinement type 1, near the feeding holes.

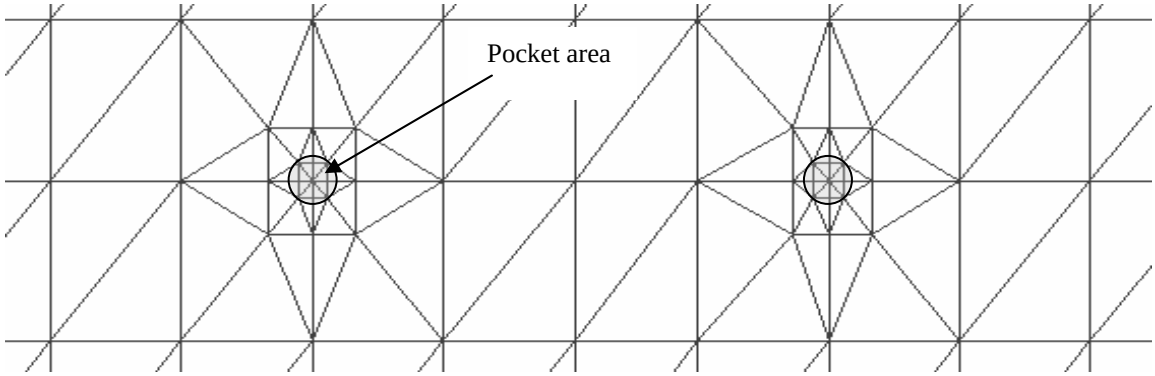

Figure 4. Mesh refinement type 2, near the feeding holes.

Once the pressure distribution is obtained, the load carrying capacity can be easily evaluated, as follows.

The total force is given by $F = \int_A P dxdy$, but for the discretized domain it can be calculated as $F = \sum_{e=1}^{Ne} F_e$, where $F_e = (P_m)_e \; A$ is the load carrying capacity of an element, *Ne* is the total number of elements and $(P_m)_e$ is the mean pressure on the element.

The total load carrying capacity of each element has two components, F_r in the radial direction and F_t in the tangential direction, and can be calculated by:

$$F_r = \sum_{e=1}^{Ne} F_e \cos\frac{(x_m)_e}{R} \qquad \text{and} \qquad F_t = \sum_{e=1}^{Ne} F_e \sin\frac{(x_m)_e}{R} \tag{12}$$

where F_e is the force acting on the element and $(x_m)_e$ is the centroid of the element.

Then, total load carrying capacity is evaluated as:

$$F = \sqrt{F_r^2 + F_t^2} \tag{13}$$

3. RESULTS AND DISCUSSION

Figure 5 (a, b and c) shows the pressure distribution around two feeding holes at the minimum film thickness position, for the three mesh types. It shows how pressure distribution changes as the mesh is further and further refined around the feeding holes. Clearly, as the mesh refinement around the feeding holes is improved, the pressure distributions changes significantly.

As can be seen in Fig. 5c, for the refined mesh type 2, the pressures at the feeding holes themselves are higher and concentrated just around the feeding holes. On the other hand, the evaluated pressures in the regions away from the feeding holes are lower and act over a larger portion of the bearing area (orange color).

In order to observe in details the pressure distribution around the feeding holes shown in Fig. 5c, an enlarged view of the pressure distribution around one of the feeding holes is shown in Fig. 6. It can be seen that the non-dimensional peak pressure (red color) is about 6.20 10^5 Pa and concentrated just at the corresponding node of the feeding hole. Meanwhile, for the standard mesh, Fig. 5a, the non-dimensional peak pressure is only about 5.80 10^5 Pa, and distributed over a larger area of the aerostatic journal bearing. It is important to observe in Fig. 5a as compared to Fig. 5c, that the pressure range in dark orange color acts over a considerable larger area, which will lead to an overestimated load carrying capacity.

It can also be seen in Fig. 6, as mesh refinement type 2 is applied, the assumption of a single node to represent a supply hole in the mesh may not adequately describe the physical phenomena, with the pocket area (dashed circle) having different pressure values. This fact contradicts the common knowledge that the pressure distribution in the pocket of the pressurized bearing can be considered constant all over the pocket area.

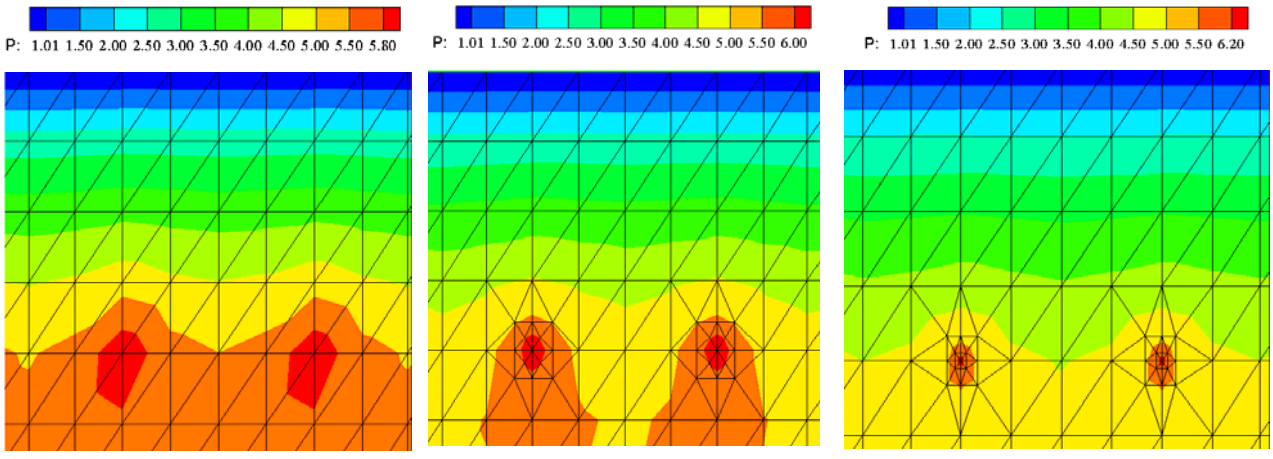

(a) Standard mesh (b) Mesh type 1 (c) Mesh type 2

Figure 5. Pressure distribution around two feeding holes, for the three mesh types.

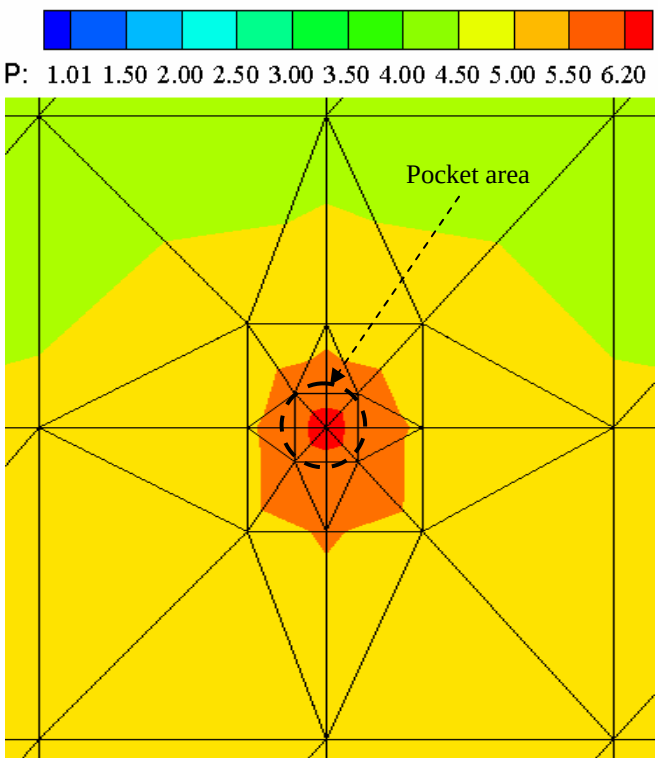

Figure 6. Enlarged view of one of the feeding holes shown on Fig. 5c.

Figure 7 shows the circumferential pressure distributions at the bearing midplane, for the three mesh types. It can be seen that the calculated pressures are significantly lower as the refinement is improved around the feeding holes. As a consequence, the effective load carrying capacity calculated by using the refined mesh type 2 may be as much as 22.45% lower than that calculated by using the standard rectangular equally spaced mesh, as shown in Tab. 3.

Table 4 shows the pressures along the bearing midplane for the three mesh refinement types. The ratios between the pressures calculated for the refined meshes types 1 and 2 relative to the standard mesh type are also given.

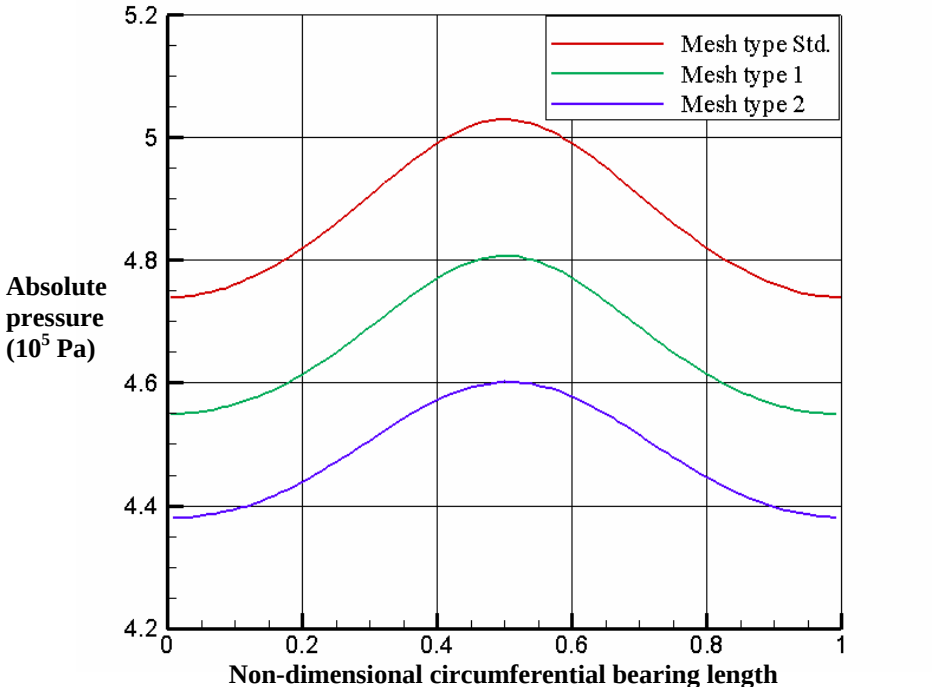

Figure 7. Circumferential pressure distribution at the middle of bearing length ($L/2$).

Table 3. Load carrying capacity versus mesh types.

Mesh types	Load carrying capacity (N)	Relative difference (%) to the standard mesh
Standard (rectangular equally spaced)	236.48	---
Refined mesh type 1	212.85	-9.99
Refined mesh type 2	183.40	-22.45

Table 4. Nodal pressures over the bearing midplane ($L/2$), at points axially coincident to the feeding holes position, for the three mesh types.

	Pressure (10^5 Pa)				
	Standard (rectangular)	Refined mesh type 1	Ratio mesh type 1 / std.	Refined mesh type 2	Ratio mesh type 2 / std.
1	4.739640	4.548721	-4.03	4.422954	-6.68
2	4.750453	4.556965	-4.07	4.430787	-6.73
3	4.781789	4.581825	-4.18	4.454641	-6.84
4	4.830703	4.623240	-4.29	4.493848	-6.97
5	4.892283	4.678508	-4.37	4.543634	-7.13
6	4.957072	4.738816	-4.40	4.594034	-7.32
7	5.008766	4.787908	-4.41	4.631826	-7.53
8	5.028872	4.807170	-4.41	4.645826	-7.62
9	5.008770	4.787915	-4.41	4.631849	-7.53
10	4.957076	4.738826	-4.40	4.594068	-7.32
11	4.892288	4.678520	-4.37	4.543667	-7.13
12	4.830706	4.623249	-4.29	4.493873	-6.97
13	4.781789	4.581831	-4.18	4.454657	-6.84
14	4.750455	4.556968	-4.07	4.430794	-6.73

Figure 8 shows the aerostatic journal bearing overall pressure distribution for standard mesh and refined mesh type 2. It can be clearly seen that the calculated pressure distribution for the refined mesh type 2 is lower than the pressure distribution calculated by using the standard mesh type, except in some nodes close to the feeding holes.

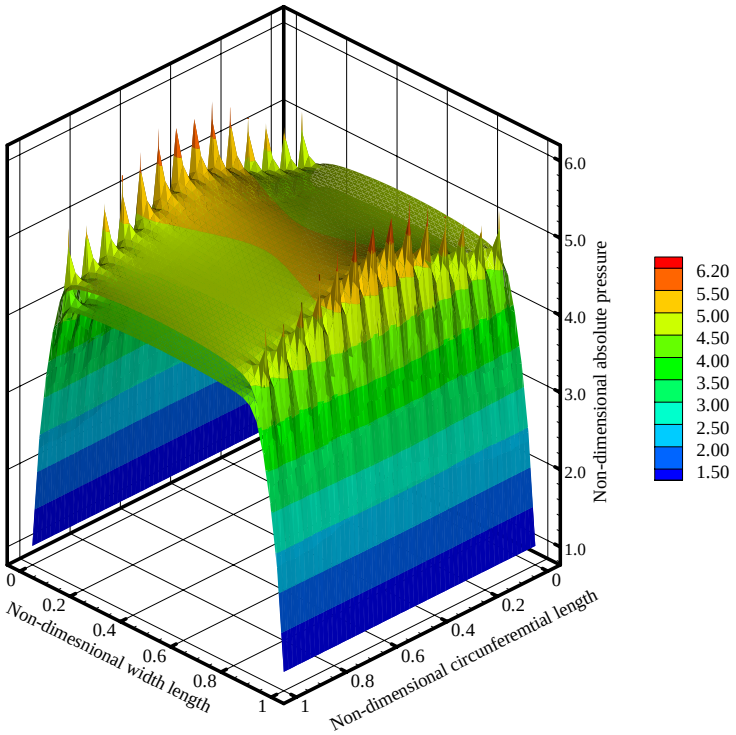

Figure 8. Comparison between the overall calculated pressure distribution for standard mesh and refined mesh type 2.

4. CONCLUSIONS

All conclusions are made by assuming that the supply hole is considered as a single node, since this assumption is considered throughout this paper. It was found that the calculated pressure distributions of an aerostatic journal bearing change significantly with mesh refinements, as shown in Fig. 5, and as a consequence the load carrying capacity too.

The circumferential pressure distribution towards the bearing mid region, calculated on the basis of the refined mesh type 2, is significantly lower than that calculated with the standard rectangular equally spaced mesh type, as can be observed in Fig. 7.

The calculated pressure distribution for the refined mesh type 2 is lower than the pressure distribution calculated by using the standard mesh type, except in some nodes close to the feeding holes. This behavior is attributed to the fact that the feeding holes are acting as punctual flow sources and the pressure gradients nearby the holes changes abruptly.

The calculated journal bearing load carrying capacity is overestimated when mesh refinement around the feeding hole is not taken into account. From Tab. 3, the theoretical load carrying capacity of aerostatic journal bearing is significantly affected by the mesh refinement around the feeding holes. Quantitatively the effective load carrying capacity may be as much as 22.45% lower than that calculated on the basis of the standard rectangular equally spaced mesh, with the pressure distribution within the pocket area taking the shape of a spike.

On the one hand, if mesh is formed by large elements and mesh refinement near the supply hole is not taken into account, the representation of a supply hole as a single node is usually accepted, since the element dimensions are bigger than the supply hole characteristic diameter itself. However, as observed above, this model would overestimate the bearing load carrying capacity. On the other hand, as long as the mesh is further refined, either globally or only in the region near the supply holes, an improvement on the evaluated bearing load carrying capacity would be expected. However, if the pocket area is not well represented by a single node, as may be seen in Fig. 6, where the pressure all over the pocket area is not constant, the proposed model would underestimate the bearing load carrying capacity. In this way, the mesh refinement type 1, seen in Fig. 5b, could be the best case to represent the real problem. This aspect will be fully analyzed in a further paper by the authors.

Although all the results concerning mesh refinement around the feeding holes reported in this paper are for aerostatic journal bearings, this important fact should be taken into account when either hybrid journal bearings or other gas bearing types are under design.

4. REFERENCES

Baker, A. J. e Pepper D. W., 1991, “Finite Elements 1-2-3”, McGraw-Hill International Editions, New York, 341 p.

B. C. Majumdar, 1980, “Externally pressurized gas bearings: a review”, Wear, 62, pp. 299-314.

Lo, Cheng-Ying et all, 2005, “Performance analysis of high-speed aerostatic bearings”, Tribology International, 38, pp. 5-14.

M. M. Reddi, 1970, “Finite element solution of steady-state compressible lubrication problem”, Journal of Lubrication Technology, july, pp. 495-503.

Powell, J. W., 1970, “Design of Aerostatic Bearing”, London, The Machinery Publishing Co. Ltd., 280 p.

S. S. Wadhwa et all, 1981, “Analysis of externally pressurized gas bearing by an incremental finite element method”, Wear, 69, pp. 133-141.

Sorin Cioc, et all, “Computation of pressurized gas bearing using the CE/SE method”, Tribology Transactions, 46, 1, pp. 128-133.

Z. Kazimierski, J. Trjnarski, 1980, “Investigations of externally pressurized gas bearings with different feeding systems”, Journal of Lubrication Technology, 102, pp. 59-64.

5. RESPONSIBILITY NOTICE

The authors are the only responsible for the printed material included in this paper.